Astrophys. Space Sci. Trans., 7, 335–344, 2011
www.astrophys-space-sci-trans.net/7/335/2011/
doi:10.5194/astra-7-335-2011

ASTRA
Astrophysics and Space Sciences Transactions

Linsley's EAS time structure method for the primary cosmic ray spectrum at LAAS

A. Iyono[1], H. Matsumoto[1], K. Okei[2], S. Tsuji[2], S. Ohara[3], N. Ochi[4], T. Konishi[5], N. Takahashi[6], I. Yamamoto[7], T. Nakatsuka[8], T. Nakamura[9], N. Ohmori[9], and K. Saito[10]

[1]Dept. of Fundamental Science, Okayama University of Science, Okayama 700-0005, Japan
[2]Kawasaki Medical School, Kurashiki 701-0192, Japan
[3]Nara University of Industry, Nara 636-8503, Japan
[4]Yonago National College of Technology, Tottori 683-8502, Japan
[5]Kinki University, Osaka 577-8502, Japan
[6]Dept. of Physics, Hirosaki University, Hirosaki 036-8561, Japan
[7]Dept. of Information and Computer Engineering, Okayama University of Science, Okayama 700-0005, Japan
[8]Okayama Shoka University, Okayama 700-86011, Japan
[9]Kochi University, Kochi 780-8520, Japan
[10]Ashikaga Institute of Technology, Ashikaga 326-8558, Japan

Received: 12 October 2010 – Revised: 18 February 2011 – Accepted: 23 March 2011 – Published: 1 September 2011

Abstract. We have installed a shift register system of extensive air show (EAS) particles in a compact EAS array built on the rooftop of the Faculty of Engineering building in the campus of Okayama University of Science and being operated since April 2006 as part of Large Area Air Shower (LAAS) experiments , in order to register each arrival time of EAS particles within 5μs. Detector simulations based on the database obtained from one of the standard cosmic ray propagation simulator in the atmosphere (AIRES) have also been carried out and the procedures to estimate the primary cosmic ray energy from the Linsley's method have been developed and examined. Applying Linsley's method to the EAS data obtained by our EAS arrays and the simulation results, we derived the energy spectrum from 10^{16} eV to $10^{19.5}$ eV. Consequently, we obtained the power-law index of $-3.2(+0.46-0.8)$ in the primary energy range of 10^{16} eV to $10^{18.5}$ eV, and obtained that a change around 10^{18} eV appeared if not taking account of the zenith angle distribution of primary cosmic rays. We compared the obtained energy spectrum with other experimental data above 10^{16} eV energies, and showed the two components of power-law energy spectra well described our data. We also showed the improvement of energy resolution by applying the restriction of zenith angle of primary cosmic rays in our simulation results, as well as the potential of the Linsley's method with a compact EAS array.

Correspondence to: A. Iyono
(iyono@das.ous.ac.jp)

1 Introduction

The cosmic ray energy spectrum compiled from different experimental approaches generally exhibits a power-law dependence on primary energy over 10 decades above about 100 GeV primary energies. The power-law index is about -2.7 below $\sim 10^{15.7}$ eV and it changes as an index $= -3.0$ above this energy. This significant change of a single power-law is called as a "knee" structure. Further, above $\sim 10^{18.7}$ eV harder energy spectrum is observed up to $10^{19.5}$ eV, which is identified as an "ankle" structure. Above $10^{19.5}$ eV, experimental data reported already are scattered between the lower energy extrapolation of energy spectrum and the theoretical prediction of Greisen-Zatsepin-Kuzmin (GZK) cutoff (Greisen, 1966; Zatsepin et al., 1966). It is reported in the recent papers (Pravdin et al., 2009; Abraha et al., 2010; Hanlon et al., 2009) that the spectra below 10^{20} eV obtained by Yakutsk (Pravdin et al., 2009), AGASA (Shinozaki et al., 2006), Auger (Abraha et al., 2010) and HiRes (Hanlon et al., 2009) experiments have a similar structure but different intensities. This discrepancy in intensities can be explained by the systematic errors in determining the EAS energy for each experimental approach. To derive the EAS energy above the ankle in these experiments, observations of both the EAS

Published by Copernicus Publications on behalf of the Arbeitsgemeinschaft Extraterrestrische Forschung e.V.

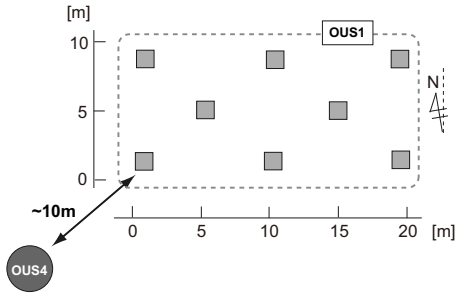

Fig. 1. The schematic top view of the OUS1 and the OUS4. The square symbols represent scintillation counters in the OUS1 array. The filled circle indicates the location of the OUS4.

core position and the number of EAS particles in the surface detector array extended to several thousand km^2 and EAS longitudinal developments in several ten fluorescence detectors have been performed.

A alternative way to derive the primary cosmic ray energy with EAS observations was invented by J. Linsley et al., on the basis of EAS particle arrival time distribution with compact EAS array experiments in 1960's (Linsley and Scarsi, 1962). In this method, an empirical formula of arrival time spread of individual EAS particles as a function of the core distance was proposed. Once the time spread of EAS particles is measured, it can provide an estimate of the EAS core distance from the compact array. The number of shower particles also provides the local particle density obtained at EAS particle counters. Therefore, the shower size n can be derived from both core distance and particle density by assuming lateral distribution function of EAS particles expected at the EAS arrays used in the experiments. The obtained shower size n can be converted into its primary cosmic ray energy by comparing EAS simulation results. The advantage of this method is to utilize compact EAS arrays for measuring primary cosmic ray energies above 10^{16} eV without extending km^2 coverage of detectors. The applications of Linsley's method in EAS primary energy determination have already been studied and discussed by Bezboruah (1996), and they concluded the spectrum became steeper around $10^{17.3}$ eV and flattered out around $10^{18.4}$ eV. They consequently insisted on the existence of the spectral break at $10^{18.2}$ eV. On the other hand, they concluded the overestimation of event rate at higher energy range due to inclusion of some delayed particles. In their theoretical estimation of the primary energy and their errors, they have not mentioned both the energy resolution depending on the zenith angles and Linsley's method dependence on the EAS zenith angle.

Linsley's method can be appropriate for the EAS events which hit the array at more than hundreds of meter core distance from the array center, because the EAS particle time spread become detectable such as more than tens of ns, and primary cosmic ray energy should also be enough to provide a number of EAS particles at large core distances. A point of controversy for applying Linsley's method in mini array experiments is that the zenith angle of EAS can not be determined for the EAS events appropriate for Linsley's method, due to the large time spread of EAS particles. Therefore we can not use typical zenith angle restriction in data selection procedures and we have to install new EAS observation system for this purpose.

In this paper, simulation studies of the application of Linsley's method by taking into account the EAS zenith angle distribution are reported as well as the results obtained by the EAS measurements and analysis in the energy range between 10^{16} eV and $10^{19.5}$ eV. Finally, we compare obtained primary energy spectrum index and its structure with other experimental data above the energy of 10^{16} eV.

2 Apparatus as parts of LAAS

2.1 LAAS

The Large Area Air Shower (LAAS) experiments have maintained eight EAS arrays scattered over in Japan since 1996, with GPS-synchronized time stamp system of which accuracy is 1μs, in order to investigate the cause of simultaneous EAS incidences detected more than 100 km baseline of EAS arrays (Wada et al., 1999; Ochi et al., 2003; Iyono et al., 2006). One of physics goals of LAAS is to explore the photo-disintegration effects of high energy cosmic ray nuclei above10^{17} eV with solar photons in the interplanetary space before cosmic ray nuclei arriving at the earth's atmosphere, which was proposed as the cue of cosmic ray composition studies above "knee" energies in 1950's by Gerasimova and Zatsepin, and recently numerical approaches potentially have also been carried out.

2.2 EAS array and shift register system

As part of LAAS EAS arrays, the four sets of compact EAS arrays are located at Okayama University of Science (OUS), Okayama city, Japan, under a mean atmospheric overburden of 1036 g/cm^2. These latitude (N) and longitude (E) are 34°42′ and 133°56′, respectively. The four EAS arrays abbreviated to OUS1, OUS2, OUS3 and OUS4 are maintained by LAAS group. To obtain EAS particle arrival timing with 5μs time window as well as the number of particles, the OUS1 is equipped with a shift register system (Okita et al., 2008). The OUS4 is installed in order to restrict EAS zenith angles. The overall sytstem and layouts of OUS1 and OUS4 have been reported and discussed in the reference Matsumoto et al. (2010).

The OUS1 consists of eight plastic scintillation counters in as shown in Fig. 1 and each counter is equipped with a scintillator of which size and thickness are 50 cm×50 cm and 5 cm respectively, and a fast photomultiplier (HAMAMATSU H7195). The detectors are deployed on the rooftop

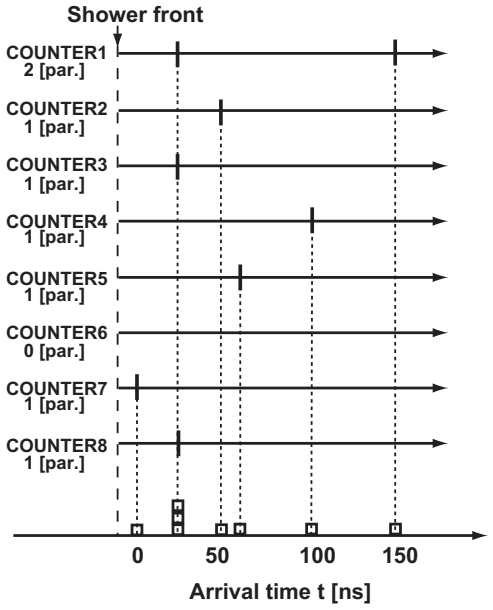

Fig. 2. The conceptual time line of arriving EAS particles at each scintillation counter recorded by the shift register (upper panel). Each black bar on the time line represents EAS particle arrival time. The particle delay histograms from trigger time (□) are shown in the bottom panel.

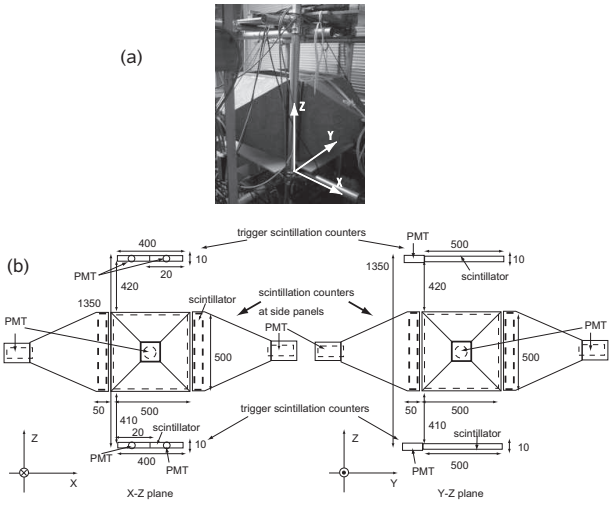

Fig. 3. The OUS4 array **(a)** and its X-Z and Y-Z views **(b)**. The unit is mm in **(b)**.

of the building in the university campus and located over an area of about 200 m^2.

The experimental data are acquired by a CAMMAC TDC (Kaizuworks Model 3781), a CAMMAC ADC (Lecroy Model 2249W), and a shift register (Mbeware Model PL-320E) when receiving the trigger request signal from the coincidence module (MPK NIM-ANY). The trigger request signal is generated when more than 3 detectors are hit within 2.5μs time window and sets the trigger time to zero second. EAS particle signals within ±2.5μs from the trigger time of zero second were recorded by the shift register system. The time stamp of triggered events is also obtained by a CAMMAC GPS timing module (Kaizuworks Model 3051A). This module maintains 10 MHz oscillator (FURUNO GT-77) synchronized with GPS 1 pps signal within 1μs accuracy and provides the EAS arrival timing in Universal Time with an accuracy of 1μs. Because correlations between arrival times and directions of EAS over the distance of more than 100km are searched in LAAS experiments (Wada et al., 1999; Ochi et al., 2003; Iyono et al., 2006), the accuracy is enough to separate the EAS events.

The EAS zenith angle θ is typically obtained by fitting a plane to the shower front of the arrival time difference which is calculated from the TDC values of EAS particles, of which resolution is set to 50ps. The angular resolution obtained by the OUS1 was estimated at about 7°(Ochi et al., 2003). The TDC can record arrival time information of the first arrived EAS particles which hit each detector within 100 ns time windows from the trigger time. Because EAS particles may be distributed up to several μs, the shift register system has been installed in the OUS1 and the OUS4 (Okita et al., 2008), in order to record the arrival time information of EAS particles detected by each scintillation counter within the time window of ±2.5μs (Fig. 2) from the trigger time. Each triggered signal of scintillation counters is digitized with the shift register system with the time resolution of 5 ns, because the shift register system is operated with a clock of 200MHz and the pulse width of the digitized signal from a CF DISCRIMINATOR (Kaizuworks Model 381) to the shift register system is set to 5 ns.

The OUS4 has been constructed in the first floor of the four stories building which is located at about 10 m distance from the OUS1, shown in Fig. 1 and Fig. 3**(a)**. At the top and the bottom layer of the OUS4, four scintillation counters, of which size and thickness are 20 cm×50 cm and 1 cm, respectively, are used in order to generate a trigger signal. And at the side panels, four sets of the same scintillation counters as the OUS1 are also installed, as shown in Fig. 3**(b)**. Those are needed to eliminate the EAS events of which zenith angles are more than 25.6°. The data acquisition system of the OUS4 is almost the same as that of the OUS1. Each EAS event is recorded by a TDC, a ADC, and a shift register when both the top and bottom counters are hit within 2.5μs. We designed the experimental set up of detectors at the OUS4 in order to select the EAS events whose the zenith angle θ should be less than 25.6°, among uniformly incident EAS events. The instrument of the OUS4, see Fig. 3**(b)**, consists of top and bottom scintillation counters in coincidence, separated by 1350 mm. The maximum zenith angle that will trigger the OUS4 depends on the diagonal length of the set of scintillation counters 640 mm and separated length of 1350 mm, and is equal to 25.6°. The time stamp of each EAS event is

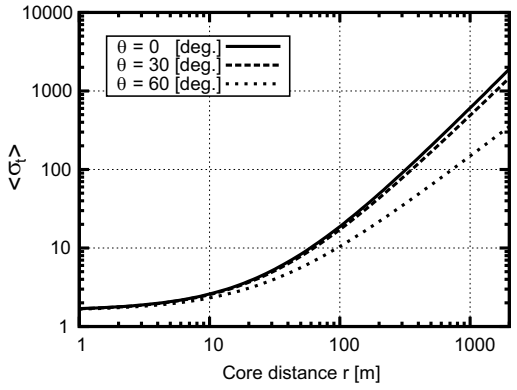

Fig. 4. The dispersion $\langle\sigma_t\rangle$ of arrival time distribution of EAS particles as a function of EAS core distance r given by Eq. (1).

obtained by a GPS timing module, and the time information between the OUS1 and the OUS4 is synchronized within 1μs accuracy.

3 Deriving core distance and primary energy

3.1 Core distance estimation

J. Linsely (Linsley and Scarsi, 1962; Linsley, 1985, 1986) found out that EAS thickness increases with the EAS core distance r, the zenith angle θ and weakly depends on the primary energy, and formulated this characteristic empirically. In reference Linsley (1986), the individual EAS thickness was defined by using the dispersion σ_t of arrival time distribution of EAS particles. σ_t is calculated by $\sigma_t = \left(\int (t-\langle t\rangle)^2 p(t)dt\right)^{1/2}$, where t is the arrival time of EAS particle and $p(t)$ is the probability density function of EAS particles arriving in time interval dt. The average behavior of dispersion $\langle\sigma_t\rangle$ can be described empirically by the following formula (Linsley, 1986),

$$\langle\sigma_t\rangle and = and \sigma_{t0}\left(1+\frac{r}{r_t}\right)^b , \quad (1)$$

where $\sigma_{t0} = 1.6$ ns, $r_t = 30$ m and $b = (2.08\pm0.08) - (0.4\pm 0.06)\,\mathrm{s}\,\theta + (0\pm0.06)\log(E/10^{17}\,\mathrm{eV})$, as shown in Fig. 4. Note that the correct b value was used in generating EAS events in the detector simulation, while the averaged b value ($b = 1.65$) obtained by calculating the zenith angle distribution of EAS was used to determine the primary energy when analyzing the OUS1 data. The contribution of third term of b was ignored. Linsley assumed the probability density function of EAS particles $p(t)$ to be a gamma distribution as $p(t) = \left(t/\mu^2\right)\exp(-t/\mu)$. If we assume a gamma distribution, σ_t is calculated by $\sigma_t = \langle t\rangle^2/2$. Actually, σ_t should be overestimated due to contamination of random noises. Then, as the standard deviation may not be the best estimator of the EAS thickness, we use the median t_{median} in the series of EAS particle arrival time as its estimator in this analysis. The relation between σ_t and t_{median} in the gamma distribution is given by

$$\sigma_t and = and \frac{\sqrt{2}}{1.67} t_{\mathrm{median}} . \quad (2)$$

r is calculated by the inverse function of Eq. (1) and t_{median} of Eq. (2) as

$$r = 30\left\{(1.35 t_{\mathrm{median}})^{(1/1.65)} - 1\right\}. \quad (3)$$

If the core distance r was determined as less than 100m, we did not use such events, because σ_t is almost constant in the region of $r < 100$ m and the relative error $\sqrt{\mathrm{variance}(r)}/r$ is almost proportional to r^{-1}. Therefore, we applied this method only for the obtained core distance $r > 100$ m.

3.2 Primary energy estimation

The OUS1 records the total number of EAS particles n by summing up EAS particles which hit each scintillation counter and registers each arrival time t_{i} ($\mathrm{i} = 1,2,\cdots,n$) of EAS particles. The particle density ρ_{obs} is calculated by $\rho_{\mathrm{obs}} = n/S$, where S is the total area of scintillation counters and $S = 2\mathrm{m}^2$. Instead of the arrival time dispersion σ_t, we calculate t_{median} value from t_{i} ($\mathrm{i} = 1,2,\cdots,n$). By substituting the t_{median} value for that of Eq. 3, we can determine the core distance r_{obs}. The lateral distribution of EAS particles have already been obtained according to the EAS simulation and the detector simulation described in Sect. 5.1. To estimate the EAS size from obtained ρ_{obs} and r_{obs}, we need the averaged lateral distribution $\bar{\rho}(r, E_0)$ integrated over the zenith angle distribution, where E_0 is the primary energy. Therefore, tables of the $\bar{\rho}(r, E_0)$ have been generated by EAS simulation. Finally, we can obtain the primary energy E_0 by comparing ρ_{obs} and $\bar{\rho}(r_{\mathrm{obs}}, E_0)$. The event selection criteria are summarized in the next section, and the simulation procedure is also described in Sect. 5.1.

4 Data set and analyses

4.1 Data set

In the OUS1 observation, the data period used for this analysis is from April 2006 to December 2008, and the total amount of observation time is 670 days. The total number of events is about 4×10^6 events and about 5×10^4 events can be used to estimate their primary energy. The corresponding event trigger rates are about 6300/day and about 75/day.

The GPS-synchronized observation between the OUS1 and the OUS4 (abbreviated to OUS1+4) started in August 2008.

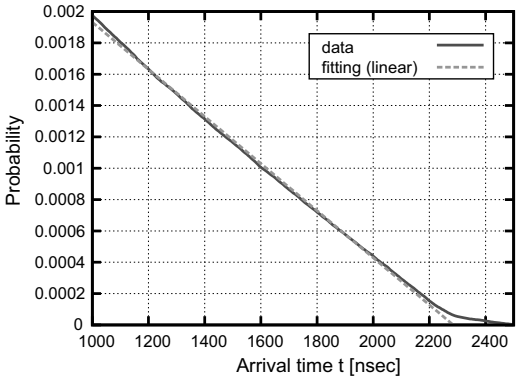

Fig. 5. The integral probability distribution $P'(t)$ of arrival time of EAS particles in the region of 1000 ns to 2500 ns, obtained by the OUS1. The solid line and the dashed line represent data and fitted linear function, respectively.

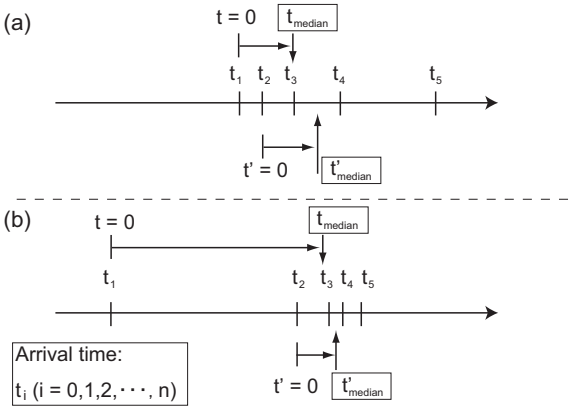

Fig. 6. The calculation method for t'_{median}. **(a)** In the case of $t'_{\mathrm{median}}/t_{\mathrm{median}} > 0.5$, we judge all of t_{i} come from EAS. **(b)** In the case of $t'_{\mathrm{median}}/t_{\mathrm{median}} < 0.5$, we judge t_1 should be a random noise, the rest come from EAS.

4.2 Estimation of random noise ratio

The observed arrival time distribution is expected to be the mixture of EAS particle density distribution $p(t)$ and random noises due to atmospheric muons or the thermal noise of the scintillation counter. The noise component should be constant per unit time. To estimate noise rate, we calculate the integral probability distribution $P'(t)$ of arrival time of obtained EAS particles as $P'(t) = \int_t^\infty p'(t')dt'$, where $p'(t')$ is the arrival time difference of obtained EAS particles. Figure 5 shows the integral distribution $P'(t)$ above 1000 ns obtained by the OUS1. Data points were fitted as a linear function from 1000 ns to 2000 ns. We have estimated contaminated noise rate as 0.4%.

4.3 Event selection criteria

The time structure of EAS particles is approximated by a relatively thin disk of charged particles that propagates with the speed of light, which is called as a shower front. Because we assume the EAS particle arrival time distribution to be a gamma distribution, there is no EAS particle which arrives at detectors before a shower front. If the random noise discussed above, appears before arrival of a shower front, there is a tendency toward increased t_{median}. Therefore, in order to minimize the contamination of the random noise, we did not use the events of $t'_{\mathrm{median}}/t_{\mathrm{median}} < 0.5$ as shown in Fig. 6**(b)**, where t'_{median} is the median value obtained from $t_{\mathrm{i}} - t_2\,(\mathrm{i} = 2, \cdots, n-1)$.

We also applied the limitation of the calculated core distance r_{obs}, if r_{obs} is less than 100 m, we did not use such events to estimate the primary energy as explained in Sect. 3.1.

5 Detector simulation of EAS arrays

5.1 Simulation procedures

In order to derive the primary energy spectrum by using the OUS1 and the OUS1+4, we estimate the acceptance, the zenith angle distribution and the energy resolution for each array by the simulation as follows.

Our detector simulation consists of the following three steps. First, by using the AIRES Sciutto (1999) which is a EAS simulation code, databases of the lateral distribution of electrons $\rho_{\mathrm{e}}(r,\theta,E_0)$ and muons $\rho_{\mu}(r,\theta,E_0)$, the number of electrons $N_{\mathrm{e}}(E_0,\theta)$ and muons $N_{\mu}(E_0,\theta)$, and the standard deviation of the number of electrons $\sigma_{N_{\mathrm{e}}}(E_0,\theta)$ and muons $\sigma_{N_{\mu}}(E_0,\theta)$ were made, where r, θ and E_0 are the core distance, the zenith angle and the primary energy, respectively. The lateral distribution of EAS particles was calculated within 2000 m radius of core distance at sea level. E_0 was sampled in the energy region of 10^{15} eV to 10^{20} eV every decade, and θ was also done from 0° to 60° every 10°. The number of EAS events generated, was one hundred at each simulation condition. The primary nuclei and hadronic interaction models were assumed to be protons and the QGSJETII-3 (Ostapchenko, 2006) and the Hillas Splitting Algorithm (Hillas, 1997), respectively.

The systematic error of energy determination came from the primary cosmic ray composition model and the hadronic interaction model. Bleve et al. (2009) reported that the QGSjet model variations were less than ±10% at core distances of 10 to 1000 m for electrons at 10^{15} eV and muons and less than 20% at 1 km core distance at 10^{19} eV. Therefore the systematic error due to the hadronic model in our simulation was estimated as less than 15%. On the other hand, for the systematic error due to the primary composition models,

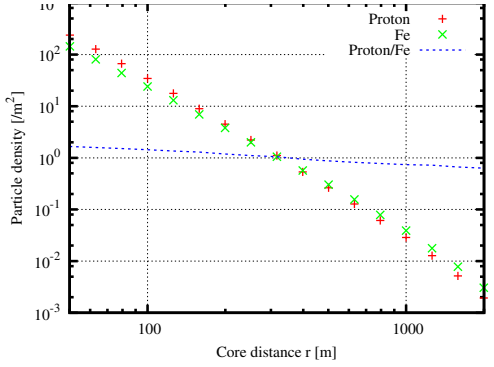

Fig. 7. The charged particle lateral distributions in proton primary case (+) and iron primary case (x) at 10^{17} eV. The dotted line represents the ratio of proton to iron primary.

Auger group has already reported in Abraha et al. (2010) that the systematic uncertainty arising from the lack of knowledge of the mass composition was about 8% at 10^{18} eV and less than 1% above 10^{19} eV. We have already studied the charge particle lateral distribution at the ground level with proton and iron primaries at 10^{15}, 10^{16} and 10^{17} eV by using the QGSjet model. The obtained charged particle lateral distribution for between proton and iron primaries was plotted in Fig. 7. When the core distance was larger than 100 m and smaller than 2000 m, these distributions were almost equal to each others. As can be seen, the ratio of proton to iron primary plotted as the dotted line in the same figure shows the weak core distance dependency. The systematic uncertainty due to the lack of knowledge of the primary cosmic ray composition is less than 25% at 10^{17} eV. By combination with these two uncertainties, the total uncertainty of our experiments was less than 30%.

Once these databases have been made, $N_e(E_0,\theta)$ and $N_\mu(E_0,\theta)$ are parameterized as $N_e(E_0,0)\cos(C\theta^a)$ and $N_\mu(E_0,0)\cos(C\theta^a)$, where a and C are fitting parameters.

Secondly, the detector simulation for each E_0 was carried out in order to make databases of the lateral distribution averaged by simulated zenith angle distribution in each array. The parameters used in this simulation are shown as follows.

1. The primary energy E_0 is sampled in the energy region of 10^{15} eV to 10^{20} eV every 0.1 decade.

2. The core distance r is sampled by a random number within 2000 m radius.

3. The zenith angle θ of EAS is sampled by a random number in the solid angle of the hemisphere within 60°. The geometrical acceptance of each scintillator which is proportional to $\cos\theta$, is taken account of.

4. The number of electrons $N'_e(E_0,\theta)$ is sampled by the Gaussian distribution of which the mean and the standard deviation are $N_e(E_0,\theta)$ and $\sigma_{N_e}(E_0,\theta)$, respectively. The number of muons $N'_\mu(E_0,\theta)$ is also calculated by the same method as $N'_e(E_0,\theta)$.

5. The particle density $\rho_e(r,\theta,E_0)$ and $\rho_\mu(r,\theta,E_0)$ are sampled by using the lateral distribution tables made in the 1st step ($\theta = 0°$ to 60° every 10°, $E_0 = 10^{15}$ eV to 10^{20} eV every decade).

6. The arrival time of each EAS particle is sampled by the random number of a gamma distribution.

7. The random noise is sampled by a random number and its rate is set to 0.4%.

The number of particle $s\rho'$ in a detector is determined by

$$s\left(\frac{\rho_e(r,\theta,E_0)N'_e(E_0,\theta)}{N_e(E_0,\theta)} + \frac{\rho_\mu(r,\theta,E_0)N'_\mu(E_0,\theta)}{N_\mu(E_0,\theta)}\right) = s\rho', \quad (4)$$

where s is a detector area $(s = 0.25\mathrm{m}^2)$, ρ' is the density of particle which hit in a detector. And, in order to take into account the contamination of the random noise in the detector simulation, the observed random noise rate of 0.4% is used, which was explained in Sect. 4.2. Noise particles are generated with a random number in the experimental time window of ±2.5μs from trigger time. We performed the array trigger so that more than three scintillators were hit by more than one EAS particle whose energy was greater than 7.5 MeV, within 2.5μs time window. Once the trigger condition was fulfilled, we calculated the number of particles and the median of the arrival time distribution obtained by summing up particles triggered in all detectors. The threshold energy of scintillation counters, 7.5 MeV, was derived by adjusting the threshold energy in scintillation to reproduce the obtained trigger rate (Ochi et al., 2003).

Thirdly, the primary energy resolution is calculated for each E_0 by using the averaged lateral distribution $\bar{\rho}(r,E_0)$ obtained above. The procedure and the parameter condition of the simulation are the same as in the second step.

5.2 Assumed primary energy spectrum

The power-law cosmic ray primary energy spectrum $f(E_0) \propto E_0^{\alpha}$ was assumed in order to carry out EAS array performance simulation. The spectral index α was sampled from −1.7 to −4.0 every 0.1 step. The observed energy spectra $f'(E_0)$ are the convolution of $f(E_0)$ with energy resolution functions and the acceptance obtained by the simulation in Sect. 5.1. The obtained $f'(E_0)$ is also described as $f'(E_0) \propto E_0^{\alpha'}$, where α' is the fitted spectral index value. We have to estimate the α value from the obtained α' value. Therefore, the accuracy of the conversion from α' to α has to be examined.

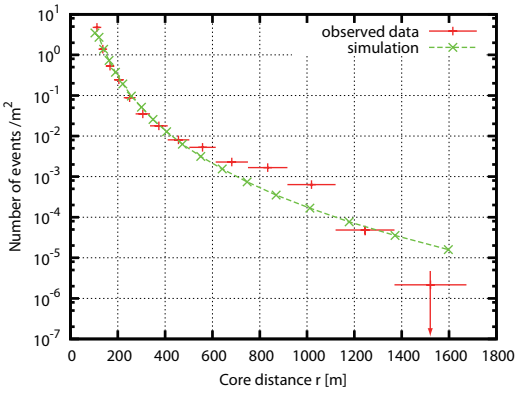

Fig. 8. The core position distributions for observed EAS and simulated one. The symbols (+) and (x) represent observed data and simulated one, respectively.

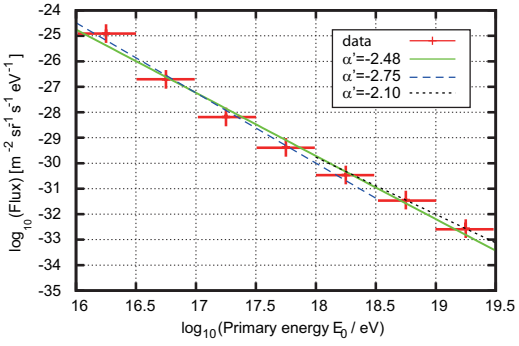

Fig. 9. The primary energy spectrum obtained by the OUS1. The symbol (+) and the lines represent data and the least square fitting, respectively.

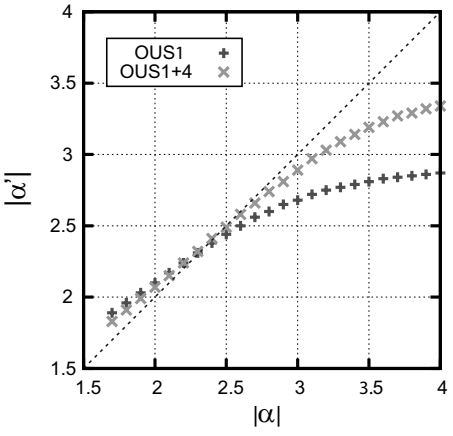

Fig. 10. The comparison between the indices of the primary energy spectra and the obtained ones.

6 Result

In order to clarify the validation of our measurement, the distributions of the determined core position and simulated one are shown in Fig. 8. As can be seen, observed data are well reproduced by the simulated one described in the section sec:sim. The event densities at the nearest and the most distant core position

The energy spectrum obtained by using the OUS1 data set is shown in Fig. 9, in the primary energy region of 10^{16} eV to $10^{19.5}$ eV. The fitting is performed with the least square fitting method. The obtained spectrum is fitted by a single power-law spectrum $E_0{}^{\alpha'}$ and the index value of the obtained spectrum α' is equal to -2.48 ± 0.12 $\left(\chi^2/\mathrm{NDF}=5.7/5\right)$. The obtained spectrum ,however, shows a gradual flattening around 10^{18} eV. We divided the obtained energy spectrum into two energy regions: (i) 10^{16} eV to $10^{18.5}$ eV, (ii) above 10^{18} eV, and fitted a single power-law to each energy spectrum in each region. The obtained spectrum indices α' in the energy region (i) and (ii) are -2.75 ± 0.17 $\left(\chi^2/\mathrm{NDF}=0.83/3\right)$ and -2.10 ± 0.08 $\left(\chi^2/\mathrm{NDF}=0.01/1\right)$, respectively. Therefore, the obtained spectrum is well expressed by two components power-law spectrum in this energy region. The intercept energy point of these two components is $10^{17.9}$ eV. The index value α of the primary cosmic ray spectrum can be obtained from the simulated relation between α and α' shown in Fig. 10. Then, $\alpha' = -2.75 \pm 0.17, -2.10 \pm 0.08$, and -2.48 ± 0.12 obtained from data are equivalent to $\alpha = -3.20(+0.46\ -0.8), -2.00(+0.12\ -0.11)$, and $-2.55(+0.19\ -0.25)$, respectively. These features of energy spectrum flattening also came from the poor energy resolution due to the zenith angle effect of shower size. We discussed the way to improve energy resolution in our experiments in the next section.

7 Discussion

7.1 Energy spectra comparison with different experiments

The structures of cosmic ray energy spectrum above the energy of 10^{18} eV such as the changes of spectral index, the energies of their break points and the existence of GZK cut off are the most important astrophysical subjects in order to explore the origins and propagation processes of ultra high energy cosmic ray nuclei in our galaxy or the external galaxies. We compared our flux data with other experiments (Fowler, 2001; Bezboruah, 1996) and Auger results (Abraha et al., 2010) in the energy range of 10^{16} eV to $10^{19.5}$ eV shown in Fig. 11, without any multiplication of the power low energy scale E. The spectral shapes of those four experiments seem generally to be consistent with each other in this energy region. The enhanced spectra above 10^{16} eV with the multiplication of flux by the energy scale $E^{2.7}$, however, shows the deviations in the spectral structures shown in Fig. 12. Our

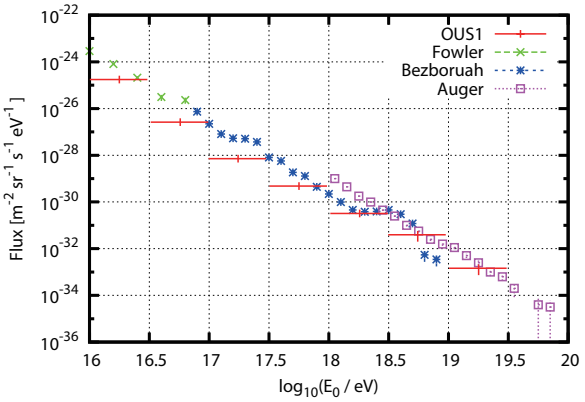

Fig. 11. The comparison of energy spectra between different experiments. The symbols(+), (x), (*), (□) represent our data, Fowler et al., Bezboruah et al. and Auger results, respectively.

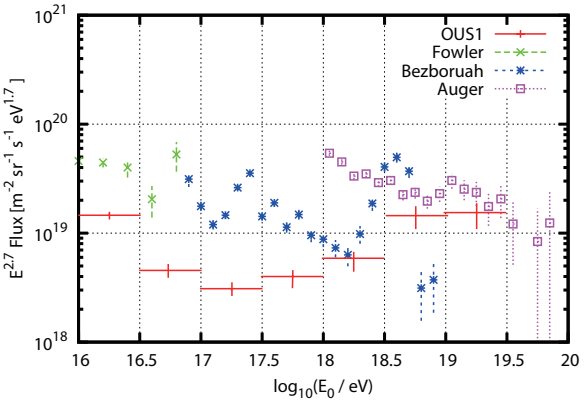

Fig. 12. The enhanced energy spectra in comparison of four experiments. The symbols(+), (x), (*), (□) represent our data, Fowler et al., Bezboruah et al. and Auger results, respectively.

absolute flux data are smaller than the others in the energy range from 10^{16} eV to 10^{18} eV. After correcting the absolute intensity of our data above 10^{16} eV by multiplying 1/0.22 derived from the expected intensity, spectral structure of our data seems to be consistent with other experiments below the energy of $10^{18.5}$ eV, shown in Fig. 13. Because of the zenith angle distribution observed at OUS1, spectral shape have shown the flattering characteristics with increasing primary energies above 10^{18} eV discussed in Sect. 7.2.

7.2 Necessity of experimental improvements for Linsley's method

The primary energy spectrum in the region above the intercept point $10^{17.9}$ eV seems to become flatter than one in the primary energy region of 10^{16} eV to $10^{18.5}$ eV, although the primary energy spectrum was assumed to be a power-law. We observed that this spectral flattening from data is caused by the accuracy of energy resolution for the OUS1. Because

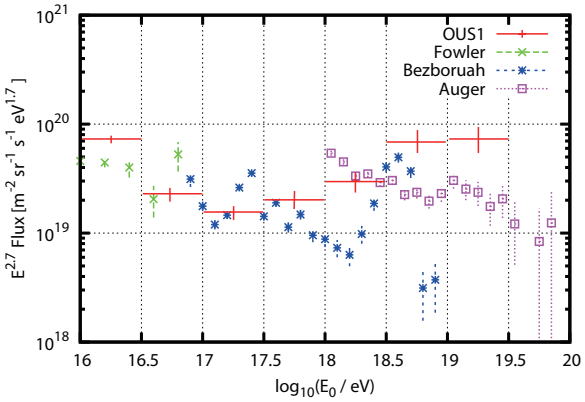

Fig. 13. The comparison of obtained primary energy spectra with the obtained ones, after correcting intensities. The symbols(+), (x), (*), (□) represent our data, Fowler et al., Bezboruah et al. and Auger results, respectively.

the OUS1 is a compact EAS array which consists of eight detectors and covers the area of about 200 m^2, it observes only a part of EAS, and it is difficult to obtain the core distance r from observing EAS particle density distribution. Therefore, we employed the Linsley's method in order to obtain the core distance r by using the OUS1. However, because the thickness σ_t of the shower front increases with the core distance r and shower front shapes are different from a flat disk, the zenith angle of EAS cannot be calculated by fitting a plane to a shower front from the arrival time of EAS particles. The size of a compact EAS array is also not enough to parameterize the shape of the shower front either by an arc or by a cone. Therefore, in the OUS1 observation, we do not obtain the zenith angle information if the core distance of the EAS is large. We have to use the mean value of the expected zenith angle distribution instead of an event by event analysis with the zenith angle information.

The systematic error for the primary energy determination mainly stems from using the mean value of b in Eq. 1 and the lateral distribution which is applied to the primary energy determination averaged by the expected zenith angle distribution. Because the systematic error of the primary energy determination can be decreased by restricting the obtained zenith angle of EAS even if the zenith angle cannot be obtained on an event by event basis, we installed the OUS4 and started the synchronized observation between the OUS1 and the OUS4. However, the acceptance of the OUS1+4 decreases as compared with one of the OUS1 due to restricting the observed zenith angle.

Figures 14**(a)** and **(b)** show the expected zenith angle distributions by using the OUS1 and the OUS1+4. Because the widths of the zenith angle distribution in the OUS1+4 become small as compared with the zenith angle distribution in the OUS1, the systematic error of the OUS1+4 with respect to the zenith angle of EAS is suppressed. Therefore,

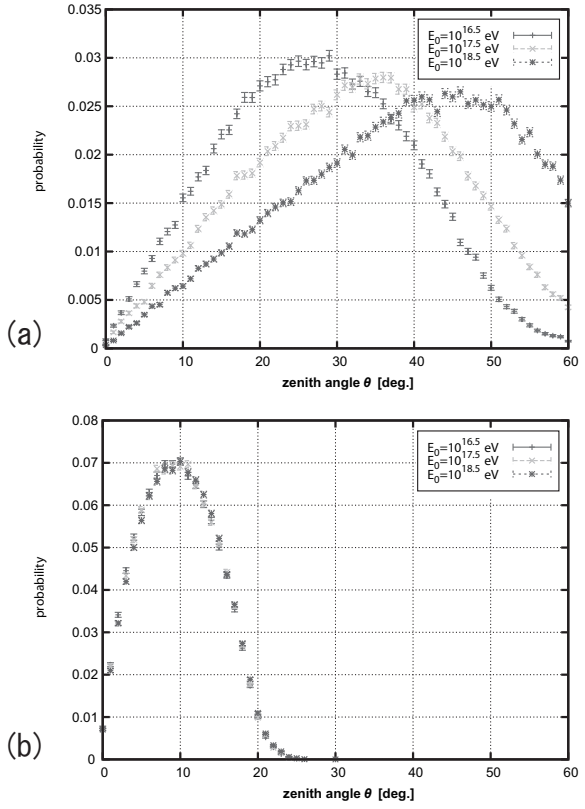

Fig. 14. The probability distribution of zenith angles observed by the OUS1 **(a)** and the OUS1+4 **(b)** for each primary energy.

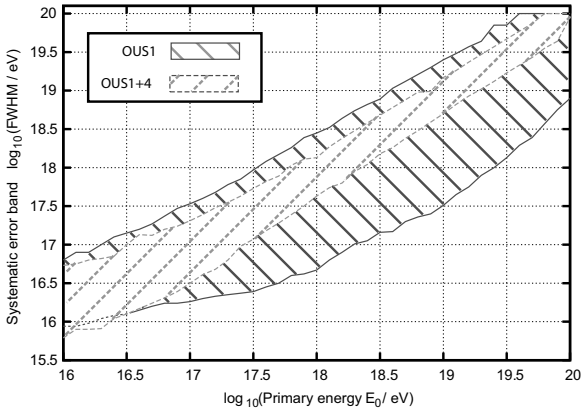

Fig. 15. The observed energy resolution as a function of primary energy E_0. The hatched area of solid line and dashed line represent the energy resolution in the case of the OUS1 and the OUS1+4 resplectively.

we can improve the primary energy resolution by using the OUS1+4. And the FWHM value of the OUS1+4 is smaller (41%) than that of the OUS1. This improvement of the energy resolution also decreases the number of events leaked toward higher energies and consequently suppresses the flattening of the primary energy spectrum. We use the FWHM value as the energy resolution and summarized the FWHM value as a function of primary energy E_0 shown in Fig. 15. The energy resolution for the OUS1+4 is much smaller than that of the OUS1 in the whole energy region from $10^{16.3}$ eV to $10^{19.9}$ eV. It is expected that the obtained change in the energy spectrum above 10^{18} eV can be resolved by the improvement of the energy resolution by using the OUS1+4, though the EAS event rate should become lower than by using OUS1 soley because of the zenith angle restriction.

8 Conclusions

The observation of a compact EAS array OUS1 equipped with a shift register system in order to record EAS particle arrival time has been carried out, and the primary cosmic ray energy spectrum above 10^{16} eV was obtained by using Linsley's method. And we also developed the simulation method by parameterizing the number of electrons and muons, their standard deviations and their lateral distributions in the EAS, and carried out detector simulations in the primary energy region of $10^{15.5}$ eV to 10^{20} eV.

In order to estimate the primary energy spectrum by using a compact EAS array, the Linsley's method is applied to estimation of the core distance. The obtained spectral index α' of the primary cosmic ray by analyzing data is equal to $\alpha' = -2.75 \pm 0.17$, and it is equivalent to a true $\alpha = -3.2$ $(+0.46\ -0.8)$. The energy spectrum obtained by OUS1 was consistent with other experiments below about 10^{18} eV energy, and some flattening of the energy spectrum was shown in our data above this energy. Even though a flattening of flux in the region above the intercept point $10^{17.9}$ eV was obtained, we cannot decide if the flattening stems from either the accuracy of energy resolution in the OUS1 observation or the change of primary energy spectrum.

The systematic error due to the primary composition uncertainty and the hadronic interaction models were estimated as about 15% and 25%, and by combination with them, the total systematic uncertainty of OUS4 array was estimated as 30%. But we need more studies the systematic errors due to primary mass composition in our simulations. Experimentally, we installed the OUS4 in August 2008 to solve this problem, because the OUS4 can reduce the systematic error. The estimated accuracy of α is expected to be improved and it enables to extend the measurable energy region to 10^{20} eV in the OUS1+4 observation. So far, the statistics of the OUS1+4 observation data is not enough to discuss the primary energy spectrum.

Edited by: T. Suomijarvi
Reviewed by: M. Pimenta and another anonymous referee

References

Abraham, J. et al. (Pierre Auger Collaboration): Measurement of the energy spectrum of cosmic rays above 10^{18} eV using the Pierre Auger Observatory, Phys. Lett. B, 685, 239–246, 2010.

Bezboruah, T., Boruah, K., and Boruah, P. K.: A non conventional method of UHE cosmic ray detection, Astropart. Phys., 11, 395–402, 1999.

Bleve, C., Parsons, R. D., Knapp, J. et al.: Systematic uncertainties in air shower measurements from high-energy hadronic interaction models, in: Proc. 31st ICRC, Łódź, 2009.

Epele, L., Mollerach, S., and Esteban, R.: On the disintegration of cosmic ray nuclei by solar photons, J. High Energy Phys., 3, 17, 1999.

Fowler, J. W., Fortsona, L. F., Jui, C. C. H. et al.: A measurement of the cosmic ray spectrum and composition at the knee, Astropart. Phys., 15, 49–64, 2001.

Gerasimova, N. M. and Zatsepin, G. T.: Splitting of cosmic ray nuclei by solar photons, ZhETF, 38, 1245–1252, 1960.

Greisen, K.: End to the Cosmic-Ray Spectrum, Phys. Rev. Lett., 16, 748–750, 1966.

Hanlon, W. F. et al. (High Resolution Fly's Eye Collaboration): Stereoscopic Measurement of the Flux of Ultra High Energy Cosmic Rays by the High Resolution Fly's Eye, in: Proc. 31st ICRC, Łódź, 2009.

Hillas, A. M.: Shower simulation: lessons from MOCCA, Nucl. Phys. B (Proc. Suppl.), 52, 29–42, 1997.

Iyono, A. et al. (Large Area Air Shower group): Energy spectrum of cosmic rays as derived from GPS-synchronized EAS array experiments, 151, 69–72, 2006.

Lafebre, S., Falcke, H., Horandel, J. et al.: Prospects for direct cosmic ray mass measurements through the Gerasimova-Zatsepin effect, Astronom. Astrophys., 485, 1–4, 2008.

Linsley, J.: Mini and super mini arrays for the study of highest energy cosmic rays, in: Proc. 19th ICRC, La Jolla, 3, 434–437, 1985.

Linsley, J.: Thickness of the particle swarm in cosmic-ray air showers, Phys. G: Nucl. Phys., 12, 51–57, 1986.

Linsley, J. and Scarsi, L.: Arrival Times of Air Shower Particles at Large Distances from the Axis, Phys. Rev., 128, 2384–2392, 1962.

Matsumoto, H., Iyono, A., Yamamoto, I. et al.: Simulation studies and implementation of Linsley's EAS time structure method for the primary cosmic ray spectrum, Nucl. Instr. Meth. A, 614, 475–482, 2010.

Medina-Tanco, G. and Watson, A.: The photodisintegration of cosmic ray nuclei by solar photons: the Gerasimova-Zatsepin effect revisited, Astropart. Phys., 10, 157–164, 1999.

Ochi, N. et al. (Large Area Air Shower group): Search for large-scale coincidences in network observation of cosmic ray air shower, J. Phys. G: Nucl. Part. Phys., 29, 1169–1180, 2003.

Okita, M., Wada, T., Yamashita, Y. et al.: Primary energy spectrum of cosmic rays obtained by arrival time spread of particles in EAS, Nucl. Phys. B (Proc. Suppl.), 175–176, 322–325, 2008.

Ostapchenko, S.: Nonlinear screening effects in high energy hadronic interactions, Phys. Rev. D, 74, 014026, 2006.

Pravdin, M. I., Dyachkovsky, N. A., and Egorov, Yu. A.: The cosmic rays energy spectrum of the Yakutsk EAS Array, in: Proc. 31st ICRC, Łódź, 2009.

Sciutto, S. J.: AIRES: A system for air shower simulations (Version 2.2.0), astro-ph, 1–216, 1999.

Shinozaki, K. et al. (AGASA Collaboration): AGASA results, Nucl. Phys. B (Proc. Suppl.), 151, 3–10, 2006.

Wada, T. et al. (Large Area Air Shower group): Observation of time correlation in cosmic air shower network, Nucl. Phys. B (Proc. Suppl.), 75, 330–332, 1999.

Zatsepin, G. T. and Kuzmin, V. A.: Upper limit of the spectrum of cosmic rays, J. Exp. Theoret. Phys. Lett., 4, 78–80, 1966.